




RESEARCH ARTICLE | FEBRUARY 02 2023

Long-term degradation of high molar mass poly(ethylene oxide) in a turbulent pilot-scale pipe flow

H. W. Müller ; L. Brandfellner ; A. Bismarck 



Physics of Fluids 35, 023102 (2023)

<https://doi.org/10.1063/5.0131410>



CrossMark



APL Energy

Latest Articles Online!

Read Now



Long-term degradation of high molar mass poly(ethylene oxide) in a turbulent pilot-scale pipe flow

Cite as: Phys. Fluids **35**, 023102 (2023); doi: 10.1063/5.0131410

Submitted: 20 October 2022 · Accepted: 9 January 2023 ·

Published Online: 2 February 2023



View Online



Export Citation



CrossMark

H. W. Müller,^{1,a)} L. Brandfellner,^{1,2} and A. Bismarck^{1,2,3}

AFFILIATIONS

¹PaCE Group, Institute of Materials Chemistry and Research, Faculty of Chemistry, University of Vienna, Währingerstr. 42, 1090 Vienna, Austria

²Doctoral College Advanced Functional Materials, University of Vienna, Vienna, Austria

³Department of Chemical Engineering, Imperial College London, South Kensington Campus, London SW7 2 AZ, United Kingdom

^{a)}Author to whom correspondence should be addressed: hans.werner.mueller@univie.ac.at

ABSTRACT

The long-term drag reduction capability of poly(ethylene oxide) with a nominal molar weight of $M_w = 4 \times 10^6$ g/mol dissolved in water was investigated in a pilot-scale pipe flow device (inner diameter of test section 26 mm) at a Reynolds number of 10^7 . A total loss of the initially high (75%) drag reduction capability was observed over a flow distance of several ~ 10 km while the molar weight of the polymer was still high ($M_w \sim 5 \times 10^5$ g/mol). Mechanical degradation in the turbulent flow as well as ageing of the polymer dissolved in water caused this loss in drag reduction capability. A simple ansatz of two independent, statistical polymer chain scission mechanisms was used to describe the polymer degradation empirically using a modified Brostow model. This empirical description was applied successfully and suggested that the polymer exhibited at least 15 cleavage points for mechanical degradation.

© 2023 Author(s). All article content, except where otherwise noted, is licensed under a Creative Commons Attribution (CC BY) license (<http://creativecommons.org/licenses/by/4.0/>). <https://doi.org/10.1063/5.0131410>

I. INTRODUCTION

Polymer drag reduction is utilized in, and investigated for, many applications such as oil transport through pipelines,¹ hydraulic fracturing,² firefighting,³ irrigation,^{4–6} heat transfer,^{7–9} sewage systems,¹⁰ and medical applications.¹¹ All of these applications aim for a high mass flow through pipes with given diameter. This requires high flow velocities corresponding to high Reynolds numbers. The Reynolds number for pipe flows is defined as follows:

$$Re = \frac{\rho Lu}{\eta}, \quad (1)$$

where ρ is the fluid mass density, L the characteristic system size, which is the inner pipe diameter R_{id} , u the cross-section averaged fluid velocity, and η the dynamic viscosity of the fluid. At Reynolds numbers above $Re \geq 2040$ (Ref. 12), which is the case for the beforehand mentioned systems, pipe flows become turbulent. Turbulence causes an energy transfer via the Kolmogorov energy cascade into small vortices where energy driving the flow is dissipated.^{13,14} This dissipation is detectible as a pressure drop downstream and attributed to frictional

resistance (drag). The energy losses due to turbulence can be as high as 90% of the energy input required to sustain the liquid pipe flow.¹⁵ Toms discovered that low concentrations (several 10–100 s wppm) of soluble, flexible, high molecular weight polymers reduce drag significantly.¹⁶ Drag reduction DR increases with increasing polymer concentration and/or polymer length^{17,18} and can be quantified in % by

$$DR = 100 \left(1 - \frac{f}{f_s} \right) \Big|_{Re}, \quad (2)$$

where f is the fanning friction factor of the polymer solution and f_s that of the pure solvent at the same Reynolds number.¹⁷ For pipe flows, the Darcy–Weisbach equation shows that the friction factor is proportional to the pressure drop Δp along the pipe of length l , which results in

$$f = \Delta p \frac{R_{id}}{2l} \frac{1}{\rho u^2}. \quad (3)$$

Up to 80% of the frictional losses can be avoided by addition of polymeric drag reducing agents.¹⁸ A full recovery to the friction of a

laminar flow is not possible for Reynolds numbers $Re \geq 3600$.^{15,19} This is attributed to an elasto-inertial instability, which becomes dominant when the Newtonian turbulence is sufficiently reduced by polymeric additives.²⁰ The interplay of polymers and turbulent flow has yet to be revealed. Several theories describe how the polymeric additives can affect turbulence. The most prominent theories assume viscous¹⁷ or elastic effects.²¹ Another element for drag reduction is a polymer-induced formation of mesoscale flow structures with shear layers close to the wall.^{22,23} On small scale, it was observed that drag-reducing polymers damp spanwise velocity fluctuations more than the streamwise ones causing flow anisotropy.²⁴ An energy transfer from fluctuations perpendicular to the mean flow into parallel ones was also detected.²⁵ More details on the proposed mechanisms of drag reduction by polymer additives are discussed in papers by Virk,¹⁸ Graham,²⁶ and Xi.²⁷

Modeling suggests the polymer becomes strongly stretched in sheared turbulent flow, especially in the near-wall region.^{28,29} Polymer stretching relates to stress in the polymer, which is able to break the polymer backbone when the induced stress overcomes locally the bond strength of the backbone. Fully stretched polymers face the highest stresses around the midpoint and will rupture there,³⁰ which is also called backbone cleavage. The location of cleavage in the backbone is referred to as breaking point. In transient turbulence, it is questionable if full polymer stretching occurs.²¹ In case the polymers are not fully stretched, a broader distribution of breaking points is possible.³¹ Experiments in turbulent pipe flow at high Reynolds number ($Re \leq 730\,000$) and small pipe diameter ($d = 0.7$ cm) demonstrated that long linear molecules break close to the mid-point, which resulted in a narrow molecular weight distribution.³² Cleavage around the midpoint due to shear stress in cross flow was observed by Odell *et al.*³³ Other experiments in pipe flow revealed cleavage points distributed along the polymer backbone.³⁴ It is inherent that the drag reduction mechanism itself causes a degradation of long chain polymers, which then loose drag reduction capability with time.^{35,36} This is a significant challenge for polymer drag reduction^{37–39} and to date focus of research.^{27,30,39,40} For the application of polymeric drag reducing agents in turbulent pipe flows, it is of importance to know the lifetime of drag reduction. The key questions are:

- how fast do polymer chains degrade?
- will the degradation come to a stop while some drag reduction capability remains?

Another important question was raised by Soares in his review on drag reducing polymers in turbulent flows:³⁰

- How does the degradation of molecular weight relate to decreasing DR?

The problem of polymer degradation might be overcome by supramolecular structures.^{27,41} Supramolecular structures consist of comparably short polymers ($M_w \sim 10^3$ – 10^4 g/mol) connected via non-covalent bonds to form chains of ultra-high molecular weight ($\sim 10^6$ g/mol), which act as drag reducing agents. Different to covalent bonds, non-covalent bonds can re-establish after breakup. Supramolecular structures are intended to scission in shear flow at the non-covalent bonds, which act as physical fuse, and this way protect the covalent backbone of the shorter subchains. In regions of reduced shear, the non-covalent bonds can reestablish. A recent investigation showed that the balance of covalent and non-covalent bond strength

in turbulent shear flow is challenging.⁴² A better, quantitative knowledge on polymer degradation will deliver valuable input to design supramolecular structures for drag reduction.

A model for the mechanical degradation of polymers by chain cleavage was developed by Brostow.³⁶ In his model, polymer degradation with time is described by

$$\frac{M_n(t)}{M_{n0}} = \frac{1}{1 + W(1 - e^{-ht})}, \quad (4)$$

where M_n is the number averaged molecular weight, M_{n0} the initial number averaged molecular weight of the polymer added to the flow, W the total number of breaking points per added molecule at infinite time, t the time elapsed since the start of the flow, and h the degradation rate constant. Brostow assumed that the approximation

$$\frac{DR}{DR_0} \approx \frac{M_n}{M_{n0}}, \quad (5)$$

holds where DR_0 is the initial drag reduction. When compared to experimental data, Eq. (4) is often used in a semi-empirical manner with W and h utilized as fit parameters.

Many studies on the mechanical degradation of polymeric drag reducing agents were performed in Couette–Taylor flow, e.g., Refs. 43–48, since the parameters can be well controlled and it is easy to perform long-term measurements in a rheometer. Experiments in rotational flow indicate some remaining drag reduction at infinite time.^{34,45–47} Data on mechanical degradation in turbulent pipe flows (e.g., Refs. 48–52) are rather scarce. This is especially true for high quality data in long-term operation and for experiments in pilot-scale devices. Pilot-scale and industrial-scale experiments are required since a size scaling for polymer degradation is not available.⁵³ Reports on the use of Brostow's model to describe polymer degradation in turbulent pipe flow in a semi-empirical manner come to inconsistent conclusions whether the model is applicable, especially if it describes the long-term behavior.^{23,52,54} Here, we have to point out that the model parameters allow for sufficient freedom to generate a wide range of slopes to describe the experimental data. A solid verification of the Brostow model can be made only when the measured DR becomes independent of residence time and stays finite. This allows to decouple h and W , which are otherwise strongly linked. We are not aware of such data for turbulent pipe flow. Observations in rotational flow can be used to understand the basic processes causing polymer chain scission, but the results from rotational flows cannot directly be transferred to turbulent pipe flows since the flow dynamics are different.⁴³

The goal of our work is to provide high-quality data on the mechanical degradation of high-molecular poly(ethylene oxide) (PEO) in aqueous turbulent pipe flow at a Reynolds number of $Re = 10^5$ in a linear pilot-scale test device. PEO is an effective nonionic drag reducing agent.^{17,18} It is cheap, nontoxic, easy-to-handle and well water-soluble at any concentration and molecular weight, even at low temperature.^{55,56} Therefore, PEO was already chosen for many previous drag reduction experiments, see, e.g., Refs. 17, 18, 23, and 45. Here, special focus is placed on the degradation rate and the long-term drag reduction toward infinite time. During our experiment, we observed both polymer M_w reduction by mechanical degradation and ageing. Both degradation processes will be discussed. The experimental data are compared to Brostow's model. Our degradation study in pipe flow was accompanied by gel permeation chromatography (GPC)

analysis to quantify the changes in the polymer molecular weight distribution. Modifications of the solution viscosity during the experiment were monitored by means of rheology.

II. EXPERIMENTAL SETUP AND METHODS

A. Flow facility ViEDRA

The long-term experiment on polymeric drag reduction in turbulent pipe flow was performed in a linear pilot-scale flow facility. The device was originally designed and operated by Zadrazil.^{23,57} It allows for Reynolds numbers up to $Re_{max} \sim 10^6$. The flow is pressure driven since mechanical pumps cause premature polymer degradation.⁵⁸ This flow facility was redesigned to minimize the number of flanges and bends. Both are expected to cause extra drag and polymer degradation. The upgraded flow facility is called ViEDRA (Vienna Experiment for Drag Reducing Agents). Its setup is schematically shown in Fig. 1. The polymer solutions are prepared in the mixing tank, which can

accommodate 350 l. From the mixing tank the solution passes a pneumatic ball valve and flows into the 300 l pressure vessel. After closing the valve to the mixing tank, the pressure vessel is pressurized by compressed air, currently up to 7 bar. The pressure vessel is connected to the straight pipe. At the beginning, the liquid passes a pipe of $R_{id} = 50$ mm inner diameter, an pneumatic ball valve, and a manual gate valve, located 105 mm upstream of the electromagnetic flow meter (Sitrans FM Magflo MAG 5000, Siemens, Denmark). After the flow meter, the pipe narrows to $R_{id} = 26$ mm. Here, a honeycomb flow straightener is inserted to homogenize the flow profile. Next is the test section, which consists of a 7200 mm long pipe without flanges and has one weld only. The first 1760 mm of the test section allows turbulent flow to develop. This distance is longer than the maximum entrance length which is required to establish full turbulence at the pipe entrance $l_h \leq 4.4R_{id}Re^{1/6} = 1144$ mm (Ref. 59). At $l = 1760$ mm the reference point for the differential pressure measurements is mounted. The

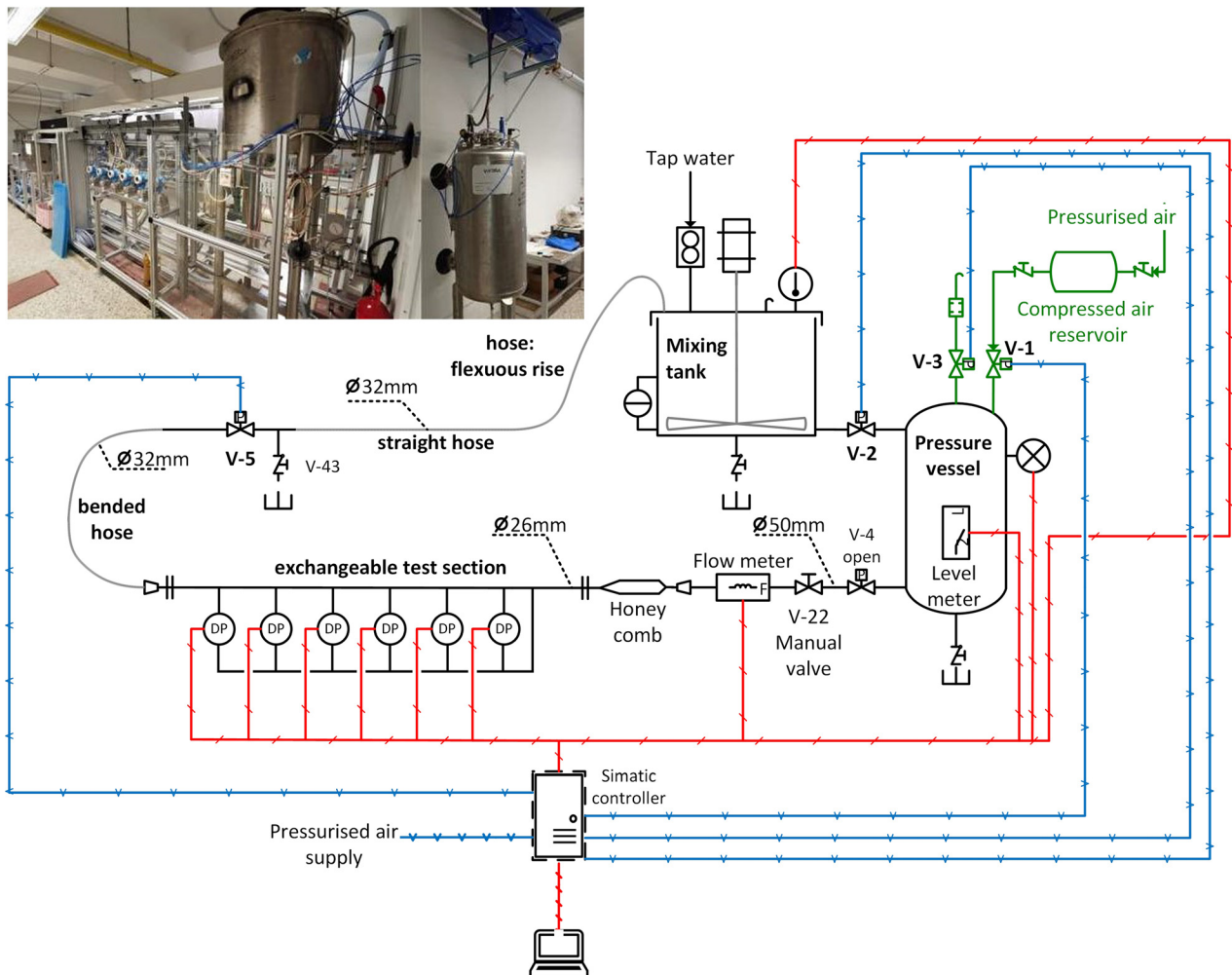


FIG. 1. Schematic outline and photograph of ViEDRA. The hand valve V22 was removed in the course of the experiments. The blue lines show the pressure lines of the valve actuators, and the red ones the connections of the sensors to the control computer. The green solid lines at the top of the pressure vessel represent pipes to pressurize and depressurize the pressure vessel.

08 January 2024 09:24:22

pressure measurements are located at $l = 1960 + n \times 1000$ mm ($n = 0-5$). The differential pressures Δp are measured using differential pressure transducers (Deltabar S, Endress & Hauser, Germany). The mean of five of these pressure drops per length is used to calculate DR . The first differential pressure is excluded from analysis since it covers a distance of only 200 mm, leading to an unacceptable signal to noise ratio. All pipes and tanks are made of stainless steel. After the test section, the liquid transits into a polyvinyl chloride hose with an inner diameter of 32 mm. The hose bends 180° upward with an average radius of 385 mm (minimum bend radius ≈ 180 mm), passes a pneumatic pinch (V5) and a manual ball valve (V43), and going quite straight back until it rises and connects to the mixing tank to close the loop.

The pressure-driven flow in ViEDRA implies an operation split into individual cycles since the pressure vessel can only be filled at ambient pressure. A cycle consists of solution transfer from the mixing into the pressure vessel, pressurizing the vessel, solvent flow through the pipe system, and finally depressurizing the pressure vessel. ViEDRA allows for feedback controlled automatic cyclic operation with a liquid flow at either constant driving pressure, flow rate or Reynolds number. The feedback control tolerates $\pm 5\%$ variations in the control parameter to avoid feedback induced oscillations in the flow. The driving pressure controller factors in the hydrostatic pressure of the fluid in the pressure vessel. In the experiments presented in this paper, the feedback control was on $Re = 10^5$. As common for pilot-scale experiments on drag reduction, viscosity changes caused by the drag reducing agents were not considered in the Reynolds number control. Viscosity variations with temperature were accounted for. The temperature measurement was located in the mixing tank.

For data analysis, the mean values of the measured quantities during the flow velocity flat top of each cycle were taken into account. For each cycle, a known fraction of the solution remained in the mixing tank and pressure vessel. Therefore, the polymer travel distance was a statistical value calculated from the loop length $l_{\text{cycle}} = 20\,450$ mm, the number of passed cycles N_{cycle} , and solution volume fraction pumped through the system within a cycle f_{cycle} .

$$d = l_{\text{cycle}} N_{\text{cycle}} f_{\text{cycle}}. \quad (6)$$

l_{cycle} was composed of 2005 mm pipe of 50 mm inner diameter, 7496 mm pipe of 26 mm inner diameter (including the straightener), and 10 949 mm hose for the backflow. Additionally, there were two free-drops of about 800 mm into the mixing and the pressure vessel for each cycle. These two free-drops were not considered for l_{cycle} since there is no wall shear stress. The different diameters over l_{cycle} cause variations in Re . The nominal parameters and control parameters were defined by the test section. The pipe sections with $R_{id} = 50$ mm were rather short. In the hose, Re was reduced by about 19% compared to the test section. Here, we have to expect the polymer degradation per distance was somewhat less pronounced than inside the test section. On the other hand, flanges, bends, valves, and the two drops caused some additional degradation. In total, the polymer degradation in ViEDRA was representative for the nominal Reynolds number. In the course of the experiments, valve V22 was removed which reduced l_{cycle} to 20 340 mm.

B. Preparation of PEO solutions

The drag-reducing agent for this study was poly(ethylene oxide) (PEO), purchased from Sigma Aldrich, with nominal molecular

weights of 2×10^5 and 4×10^6 g mol⁻¹, respectively. The polymers were used as received.

All polymer solutions had a concentration of 100 wppm and were prepared following the same recipe. The polymer powder was added at room temperature to tap water in the ViEDRA mixing tank within a time window of 30 min. In this time window, the impeller of the mixing tank was running at 60 rpm to avoid macroscopic aggregation. Afterward, the polymer was left to dissolve for another 24 h without mixing to minimize mechanical impact. In total, three solutions with PEO of a nominal molecular weight of $M_w = 4 \times 10^6$ g mol⁻¹ (labeled 4E6-1, 4E6-2, 4E6-3) and one solution with $M_w = 2 \times 10^5$ g mol⁻¹ (labeled 2E5-1) were prepared. After operation breaks over night or over the weekend, the solutions were stirred at 60 rpm for 1 min to homogenize the solution and to remove aggregates.

C. Gel permeation chromatography to follow polymer degradation

Information on the molecular weight distribution of the dissolved polymers was gathered by gel permeation chromatography (GPC, Viscotek TDA 302, Malvern Panalytic). Details on the measurements can be found in the [supplementary material](#). Solution samples from ViEDRA were taken every morning and after selected runs. They were stored for analysis at ambient temperature in the dark. Several samples were analyzed multiple times over a period of up to 50 days. We focused on the weight averaged molecular mass M_w , which is quite resilient against baseline drifts in the refractive index detector (about 3% error for a 10% drift⁶⁰).

D. Rheological characterization of polymer solutions

Additionally, rheological characterization of the ViEDRA samples was performed using a rheometer (Discovery HR-2, TA instruments), which was equipped with a double gap geometry. Details on the geometry and experimental procedure are listed in the [supplementary material](#).

Shear rate ($\dot{\gamma}$) scans covered the azimuthal laminar flow (Couette) regime and the Taylor flow regime in the outer gap. In the Taylor regime, vortices perpendicular to the angular flow occur in the outer gap while the inner gap stays in the Couette regime at all times.⁶¹ This transition becomes visible by a change in slope of the apparent viscosity as function of shear rate $d\eta_{\text{app}}/d\dot{\gamma}$. For the Couette regime, we found in shear rate scans typical variations in η_{app} of $\leq 5\%$ comparable to variations of η_{app} for Newtonian fluids in the range of 1%–3%. Therefore, the viscosity was considered to be constant over the whole Couette regime.

It is possible to derive the apparent viscosity at Taylor flow onset η_{on} from the angular velocity at onset ω_{on} ,⁴³

$$\left(\frac{\rho\omega_{on}}{\eta_{on}}\right)^2 = \frac{\pi^4(\delta + 1)}{2(\delta - 1)^3 R_3^4} F_0, \quad (7)$$

with the aspect ratio $\delta = R_4/R_3 \approx 1.057$ of the outer stator radius R_4 over the outer rotor radius R_3 , and the geometry factor F_0 ,

$$F_0 = \frac{1 - 0.652(\delta - 1)}{0.00056 + 0.0571[1 - 0.652(\delta - 1)]^2}. \quad (8)$$

For dilute, low-viscosity aqueous polymer solutions we found the absolute value of η_{on} with a typical relative error of $\approx 1\%$ to be more robust than η_{app} with a relative error of $\sim 10\%$. Therefore, the zero shear viscosity η was approximated using η_{on} [Eq. (7)].

With this method, η was determined for all ViEDRA samples [$\eta(\text{sample})$] as well as for the pure solvent η_{ref} and the relative viscosity was calculated,

$$\eta_{rel} = \frac{\eta(\text{sample})}{\eta_{ref}}. \tag{9}$$

All samples were characterized at $T = 25^\circ\text{C}$. For some samples of the ViEDRA solutions, 4E6-2 and 4E6-3 and pure water additional measurements were also made at 21.4 and 21.8°C , which allowed to verify that η_{rel} was almost temperature independent in the range $21\text{--}25^\circ\text{C}$ covering the solution temperature variations in ViEDRA when performing the experiments.

E. Reference data

Prior to flow tests, solution samples were taken from the mixing tank to determine the initial molecular weight of the dissolved polymers. The weight-averaged molecular weights from GPC measurements compared to the nominal ones are listed in Table I.

The fanning friction factor of water f_s as function of Re was measured in ViEDRA prior to pumping the PEO solutions through the device. These data were fitted by a polynomial to provide f_s for any Re . The fit function was

$$f_s = 6.96886 \times 10^{-14} Re^2 - 2.39488 \times 10^{-8} Re + 0.00629604. \tag{10}$$

So, f_s is decreasing with increasing Re for the Re range of interest (see also Fig. S2 in supplementary material).

III. EXPERIMENTAL OBSERVATIONS

A. Global drag reduction evolution

Figure 2 presents DR as function of traveled distance for three long-term experiments. Up to ~ 3100 runs were performed and lasted up to 51 days. The initial nominal molecular weight of the polymer was $M_w = 4 \times 10^6$ g/mol and the solution's polymer concentration 100 wppm. The dataset was restricted to runs with $94000 < Re < 102000$, and each data point represents one run. The viscosity of pure water η_{ref} was used to calculate Re . This is quite common when analyzing polymeric drag reduction in pipe flows, see e.g., Ref. 62. The solution's viscosity η is up to $\sim 20\%$ higher than η_{ref} . This difference causes a small error when calculating DR and vanishes with chain scission. The maximum absolute error was found to be less than 2% in

TABLE I. Initial weight averaged molecular weights of the dissolved polymers. Nominal values from provider and initial GPC data are shown.

Experiment	Nominal, M_w (g/mol)	M_w from GPC (g/mol)
2E5-1	0.2×10^6	0.09×10^6
4E6-1	4×10^6	2.9×10^6
4E6-2	4×10^6	2.7×10^6
4E6-3	4×10^6	3.1×10^6

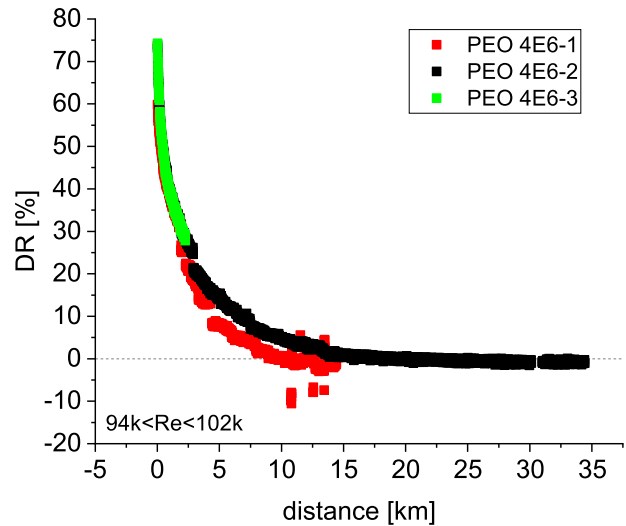


FIG. 2. DR as function of travel distance for three 100 wppm polymer solutions of PEO with a nominal molecular weight of $M_w = 4 \times 10^6$ g/mol.

DR (Fig. 5). Experiment 4E6-1 suffered from extra noise caused by valve V22, which was removed before experiments 4E6-2 and 4E6-3 were performed. The DR data exhibit several drops at constant distance, which coincided with operation breaks over the weekend when the polymer solution was at rest. We attributed this drop to polymer ageing, which we define as polymer scission in solution that is not generated by shear forces. Most publications on polymer solution ageing discussed polymer aggregation⁶³ or attributed changes in the viscoelastic behavior to disentanglement of polymer aggregates.^{64,65} However, other previous publications reported a reduction in the polymer's molecular weight over time.⁶⁶ Aggregates that might form in the resting solution overnight were assumed to breakup when the solution was stirred prior to operation. Therefore, they were not expected to play a significant role in the experiments presented in this paper.

In the beginning, DR of up to 75% was obtained, followed by a steep exponential drop. Finally the drag reduction vanished completely after 10–20 km and DR became slightly less than zero, which will be discussed later. These results were reproducible. Toward longer distances, DR in the experiments 4E6-1 and 4E6-2 started to differ. This can be attributed to different solution ages at the same distance traveled. Experiment 4E6-1 took longer than 4E6-2 to reach the same distance.

For comparison, the experiment was repeated at the same polymer mass concentration of 100 wppm but reduced molecular weight of nominal $M_w = 2 \times 10^5$ g/mol (experiment 2E5-1). The polymer solution was followed over a distance of ~ 1 km corresponding to 130 runs. In this experiment, no DR was observed.

B. PEO molar weight, degradation, and ageing

Figure 3 shows M_w of nine samples taken from ViEDRA over the course of experiment 4E6-2. The samples were not only characterized immediately after being taken from ViEDRA but repeatedly over a time span of up to 50 days after removal. The data reflect the

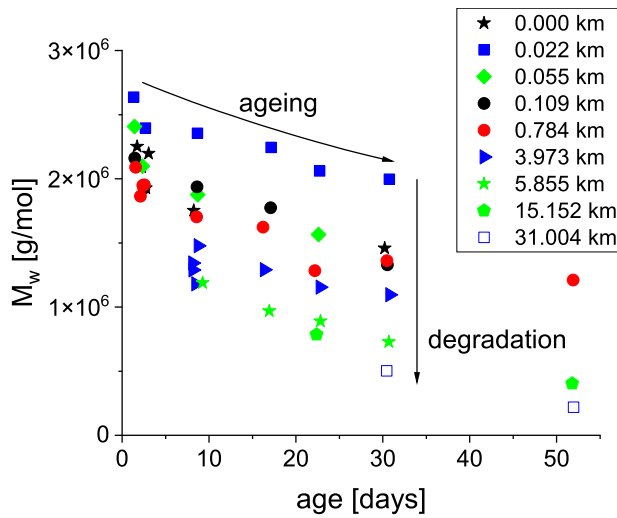


FIG. 3. Molecular weight M_w as function of age and distance. Data from the experiment 4E6-2. The age is measured relative to the time of polymer dissolution. The color/symbol code indicates the distance the polymer traveled in ViEDRA before the molar weight was characterized by GPC.

mechanical degradation of the polymer in shear flow visible as decrease in M_w with traveled distance, but also a decrease in M_w with time at rest, caused by polymer ageing. Like shear-induced degradation, ageing seems to slowdown with decreasing M_w possibly toward an asymptotic value. The reduction in M_w with distance traveled reveals the connection of M_w and DR . Somewhat unexpected was that M_w for a distance of $d = 0.022$ km being larger than M_w in the beginning. This might be related to an improved dissolution and homogenization after the first runs in ViEDRA, but can also be an artifact.

The development of the relative viscosity η_{rel} with respect to the viscosity of pure water is shown in Fig. 4. With increasing travel distance, both M_w and the relative viscosity decreased.

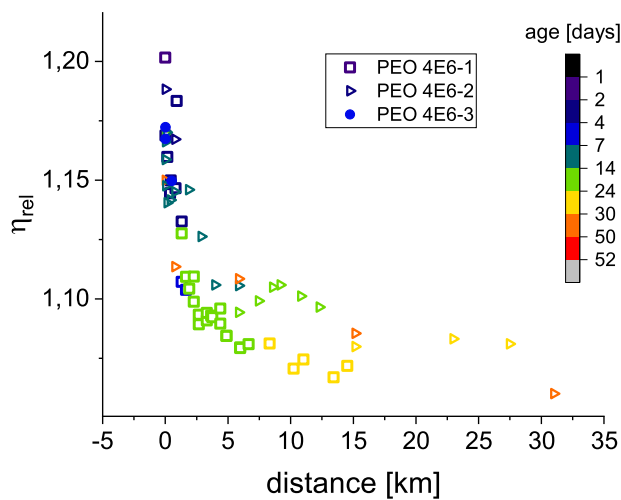


FIG. 4. Development of $\eta_{rel} = \frac{\eta_{(sample)}}{\eta_{ref}}$ [Eq. (9)] over traveled distance. The polymer solution's age is color coded.

IV. DISCUSSION

A. Influence of solution viscosity on DR

Solution viscosity changes due to polymer addition and polymer degradation have been neglected when calculating DR , where only the temperature dependent viscosity of water (η_{ref}) entered. The quality of this simplification was analyzed in a reevaluation of the drag reduction. For experiment 4E6-2, we performed a second analysis incorporating the viscosity change and compared the revised DR_η to DR estimated using the standard procedure. The fanning friction factor used to calculate DR was determined applying the Darcy–Weisbach equation [Eq. (3)]. In these equations, the viscosity η does not enter explicitly, but η influences Re and, therefore, f_s which has to be measured at the same Re as f . When η increases, all other parameters remain constant Re decreases [Eq. (1)]. In our experiment, the corrected Re_η is about $\sim 10\%$ lower than Re used for the standard analysis inserting the viscosity of pure water in Eq. (1). Therefore, f_s has to be taken at reduced Reynolds number compared to standard analysis. This results in an increase in f_s [Eq. (10), Fig. S2 in the supplementary material]. From Eq. (2), it becomes obvious that a larger f_s leads to an increase in DR_η compared to DR .

Rheometer measurements were performed to determine the viscosity of the polymer solution in ViEDRA. In the course of the long-term experiments samples were taken and η_{on} [Eq. (7)] of these samples determined. The correction factor $\eta_{rel} = \frac{\eta_{on}}{\eta_{ref}}$ was then used to derive the precise values of the Reynolds number $Re_\eta = Re/\eta_{rel}$ and drag reduction DR_η . Figure 5 shows there is only a slight increase in drag reduction with the correction by 1–2% in absolute numbers. This difference is not substantial considering the DR capability of the PEO solutions. However, it is of interest when discussing the long-term behavior of polymeric drag-reducing agents. The standard analysis using η_{ref} delivers DR slightly less than zero. Using the actual solution viscosity yields

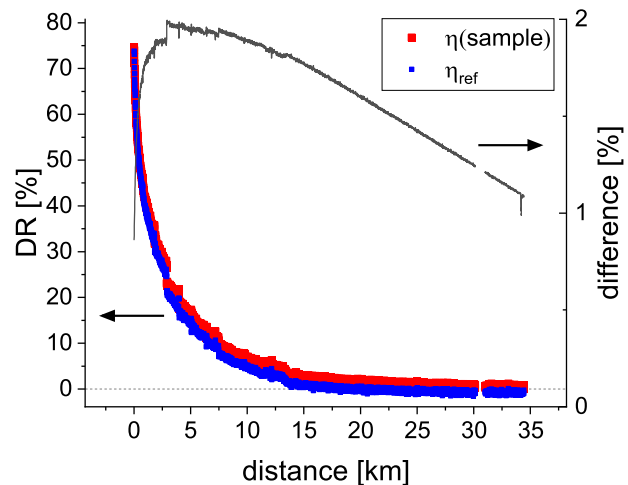


FIG. 5. DR calculated applying the viscosity of pure water in blue (η_{ref}) and DR_η using the real viscosity of the polymer solution in red [$\eta_{(sample)}$]. Measurement data taken from 4E6-2. The black solid line represents the absolute difference $DR_\eta - DR$.

$$0 < \lim_{d \rightarrow \infty} DR < 0.2 \dots 0.4 \%, \quad (11)$$

for experiment 4E6-2. This is a remarkable precise confirmation of the total loss of drag reduction. DR is reduced by a factor of ≈ 200 compared to its initial value.

B. Empirical description of PEO ageing

A detailed description of ageing is beyond the scope of this paper, but disentangling ageing and degradation is required to compare the experimental data of DR to Brostow's model. In Secs. IV B and IV C, we will discuss the development of the molar weight in the experiment, starting with the ageing process. Our investigations showed that light, pH, and dissolved oxygen promote PEO ageing in aqueous solutions. For the experiments presented in this paper, ageing by light is negligible. It is predominantly driven by hydronium ions (see also supplementary material). Already mentioned was the slowdown of ageing with time. Therefore, we assumed a modified exponential decay of M_w with t_d , which shows an increasing half value time with decreasing M_w . The most reliable GPC data of M_w stemmed from experiment 4E6-2. All available M_w measurements for ten different flow distances between $d = 0.0$ and 12.3 km were fitted together using a nonlinear fit applying the Levenberg–Marquardt algorithm in OriginPro,[®]

$$M_w = M_{w0} e^{-\frac{1}{c} \left(\frac{t_d}{t_d}\right)^b}, \quad (12)$$

with the fit parameters being M_{w0} and c . The decay parameter c is shared by all datasets. M_{w0} is fitted individually to each flow distance, which reflects the degradation in the turbulent flow with distance traveled through the device. The parameter b is varied on a fit to fit base from 0.1 to 0.8 and was kept constant during the fit to avoid overparametrization. t_d is the time elapsed since the polymer was added to the solvent, measured in days. The best fit was obtained with $b = 0.2$, but $0.15 < b \leq 0.4$ delivers fits of comparable quality. Further fit details are presented in the supplementary material.

Figure 6 shows all data from experiment 4E6-2 used for the empirical ageing fit. Most of them were already included in Fig. 3. M_w is plotted on logarithmic scale and t_d with the power of 0.2. The linear trend of the datasets supports the plausibility of the applied fit. Nevertheless, it seems the fit underestimates the M_w decrease for the lowest M_{w0} . Possibly, the half value time of ageing depends on polydispersity, which will depend on the travel distance in ViEDRA, causing for $d > 10$ km a faster ageing (larger b) than at shorter flow distances. However, the database is too weak to verify such an accelerating process with increasing distance and has to be addressed in later studies.

Since ageing was expected to be a stochastic process an exponential decay of the molecular weight was estimated. Our data showed an additional slowdown of the ageing which was captured by the parameter $b < 1$. This additional slowdown might be attributed to the molecular weight distribution. The weight distribution is expected to become narrower while ageing, since especially long polymer chains are prone to ageing. This narrowing already would cause a decrease in M_w beyond the reduction in M_n .

C. Does the Brostow model explain the shear-induced degradation?

The model of Brostow³⁶ postulates statistical breaking of the polymer backbone as we also assumed for the ageing process. Most

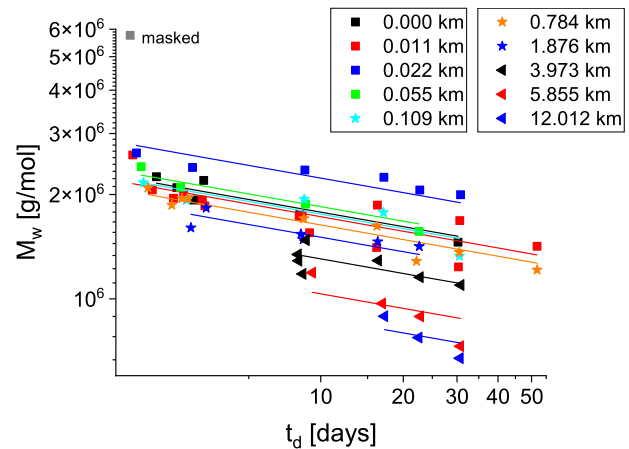


FIG. 6. The graph shows the M_w decrease in PEO over time after the solution has been taken from ViEDRA at various flow distances. This is ageing: degradation without shear stress applied. The symbols correspond to M_w determined by GPC. The solid lines show the fit according to Eq. (12) with $b = 0.2$. M_w is plotted on a logarithmic scale while t_d is plotted with the power of 0.2.

probably, these two processes will influence each other but to first order we consider them to be independent. GPC delivers $M_w(d, t_d)$, which is the weight-averaged molecular weight affected by mechanical degradation and ageing. For independent statistical degradation and ageing, we can write

$$M_w(d, t_d) = M_{w,c}(d) e^{-\frac{1}{c} \left(\frac{t_d}{t_d}\right)^b}. \quad (13)$$

Since ageing is now decoupled, $M_{w,c}(d)$ depends on the flow distance only. $M_{w,c}(d)$ is the molecular weight as it would be measured for the hypothetical case that the long-distance experiment is performed instantaneously. $M_{w,c}$ shows the effect of mechanical degradation and can be represented by Brostow's model if applicable. The relation of DR and M_w is treated separately in Sec. V. Brostow derived his model for M_n . It is presumed that the polydispersity is not varying strongly and the M_n degradation is represented by M_w data, which are much more robust.⁶⁰ Combining Eq. (13) and Brostow's model results in

$$M_w(d, t_d) = M_{w0} e^{-\frac{1}{c} \left(\frac{t_d}{t_d}\right)^b} \frac{1}{1 + W(1 - e^{-hd})}. \quad (14)$$

This equation with two independent variables t_d and travel distance d [Eq. (6)] was fitted to the experimental data using the Levenberg–Marquardt algorithm in OriginPro[®]. The empirical fit parameters were the initial molar weight M_{w0} , the number of breaking points W , and a characteristic inverse decay length h . The paired parameters for ageing b and c were taken from the ageing fit and were varied on a fit to fit base between $0.1 \leq b \leq 0.8$ to avoid overfitting. The datasets 4E6-1 and 4E6-2 were fitted together. It has to be pointed out that the parameters b and c of the ageing correction were determined from 4E6-2 only but were applied to both datasets since ageing was expected to be a universal process, which depends on the polymer solvent system only. The fit results for different ageing parameters b were compared in OriginPro[®]. The best fit for both datasets was achieved with $b = 0.4$. Again, the range $0.2 \leq b \leq 0.5$ delivered

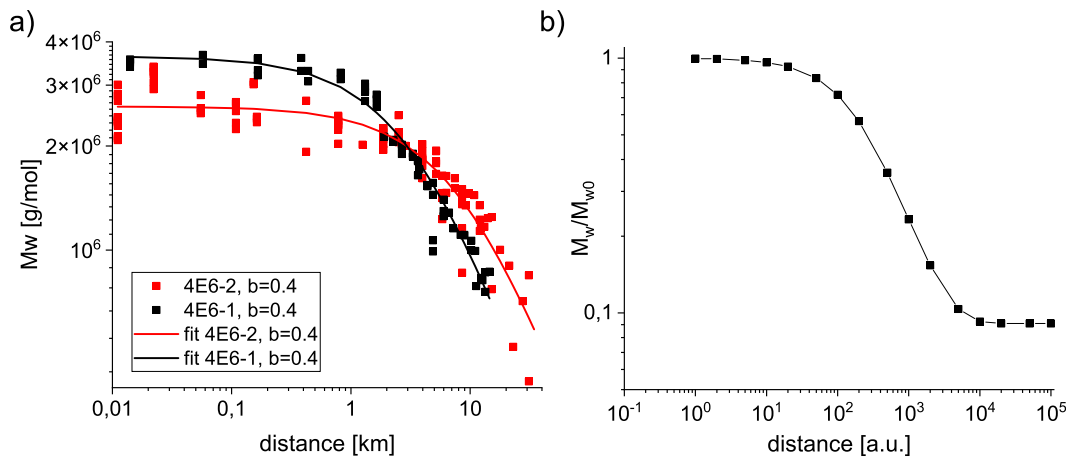


FIG. 7. (a) The age corrected weight averaged molar weights $M_{w,c}(d)$ from experiments 4E6-1 (black squares) and 4E6-2 (red squares) are plotted in comparison with the fitted Brostow function $M_{w0} \frac{1}{1+W(1-e^{-hd})}$. The age correction was performed with $b = 0.4$ [see also Eq. (14)]. The experimental data are well represented by the fitted functions. (b) Generic Brostow function given by Eq. (4) for $W = 10$.

results of similar quality as visible in the flat minimum of the Bayes information criterion (see [supplementary material](#)). Therefore, the slight shift in the optimum b compared to the ageing fit presented in Sec. IV B was within the error of the analysis. This justifies the assumption that ageing and degradation are indeed independent processes, at least to first order. The best fit to the data of 4E6-1 and 4E6-2 is plotted in Fig. 7(a). In this plot, the fit's Brostow part of Eq. (14) $M_{w0} \frac{1}{1+W(1-e^{-hd})}$ is compared to the ageing corrected molar weight $M_{w,c}(d)$. Both datasets, 4E6-1 and 4E6-2, are well represented by the fit. The fit parameters are summarized in Table II. The corrected $R^2 \geq 0.9$ indicates a good fit quality. The results for M_{w0} are good. For 4E6-2, the fit parameter M_{w0} matches the measured value well. The fit value of 4E6-1 overestimates M_{w0} compared to the initial measurement (see also Table I). It is surprising that W differs so much for the two fits. However, the parameters W and h show a significant indeterminacy, which was also flagged by the fitting software. The software also indicated that for both datasets 4E6-1 and 4E6-2 the fit parameters W and h were strongly coupled. Nevertheless, the fit function is

TABLE II. Parameters of the best fit with Eq. (14). "std err" is the standard error of the fit parameter.

Sample	Unit	4E6-1	4E6-2
M_{w0}	10^6 g/mol	3.63	2.60
std err	10^6 g/mol	0.04	0.04
W		4424	54
std err		1.6×10^{6a}	576^a
h	km^{-1}	6.25×10^{-5}	1.9×10^{-3}
std err	km^{-1}	0.022^a	0.020^a
R^2		0.979	0.907
corr. R^2		0.969	0.905

^aThis standard error reflects a possible variance in W and h while receiving a fit compatible to the experimental data. Additional physical constraints apply, which are discussed in the text.

not over-parameterized as the closeness of R^2 and corrected R^2 indicates. Albeit the chosen three-parameter fit function delivered coupled parameters, it remained our first choice to describe mechanical polymer degradation. To our knowledge, the function suggested by Brostow is the only one with a physical meaning of the parameters and, therefore, used until it is proven to be wrong or a better motivated function is available. Figure 7(b) shows how W and h decouple. Brostow's function describing the degradation reaches a constant value for infinite distance, which fixes the number of breaking points W and decouples W and h . In the experiments described in this paper, DR vanished, but M_w was still decreasing without sign of a second curvature change in the log-log plot inhibiting to decouple W and h . Here, we have to stress that the standard error given in Table II is not caused by a deviation of the fit function from the data points, but is determined by the variance produced by W and h being coupled. From the parameters in the fit to 4E6-2, we see that the number of breaking points is $W + \text{stderr}(W) = 630$ at maximum, which has to be compared to an average number of 59 000 repeat units in the polymer in the beginning. From this we deduced a typical minimum residual molecular weight at the end of mechanical degradation of $M_{w,\infty} \geq 4100$ g/mol. The residual molecular weight is expected to be a universal characteristic value for fixed Re , R_{id} , polymer concentration, and polymer and, therefore, expected also to apply to 4E6-1 while the fit to 4E6-1 does not deliver any constraint in W .

In literature, the degradation analysis is usually performed on DR instead of M_w assuming $M_w \propto DR$. We are not aware of any publication unequivocally proving that in the case of turbulent pipe flows DR degradation shows a change in curvature in the $\log DR = f(\log d)$ plot toward an asymptotic limit—or that this was even observed for M_w . This has an important implication. Without good data on the final asymptotic value, W cannot be pinned down and the parameters W and h remain strongly coupled. This coupling of W and h basically inhibits to prove Brostow's idea that the breakup process comes to a stop. The fit to 4E6-2 at least complies with his idea of a residual $M_{w,\infty}$.

We also tested for a lower limit in W using repeated fits with restricted W applying the fit function defined by Eq. (14), b was set to

0.4. These models have been compared to the best fit. The Bayesian information criterion shows a significant decrease in the fit quality for $W \lesssim 15$, clearly favoring $W > 10$ and excluding $W \lesssim 5$ (see [supplementary material](#) for details). With the fit parameter $M_{w,0}$ and the lower limit $W = 15$, the upper limit for the molar weight at the end of the experiment 4E6-1 becomes $M_{w,\infty} \leq 2.4 \times 10^5$ g/mol [see also [Fig. 7\(b\)](#)] and the measured $DR \approx 0$. This was in agreement with the observation that for sample 2E5-1 no drag reduction was observed.

Since in our experiments on PEO degradation in turbulent pipe flow DR was completely lost before the polymer chain scission came to an end, Brostow's model is not applicable in one point: with $DR = 0$ for finite M_w and, therefore, finite M_n , the proportionality of $M_n \propto DR$ cannot be generally valid. At least there has to be a threshold in M_n before DR becomes different from zero. Furthermore, in our experiments one of the main characteristics in Brostow's model was not observed: polymer degradation did not stop toward large flow distances. Nevertheless, the fit function derived by Brostow [Eq. (4)] can still be applied as empirical fit function to describe degradation even in combination with polymer ageing. For one of our datasets, the fit suggests that the mechanical degradation of the polymer chains will end with a residual chain length of about 100 repeat units as a lower boundary, which is expected to be a universal behavior for our experimental system. The difference in the polymer behavior in the datasets Brostow referred to in Refs. 36, 67, and 68 and the observations presented in this paper become obvious in the parameter W . This parameter is $0.5 < W < 6$ in all datasets Brostow analyzed (including 7.1×10^6 g/mol polystyrene in toluol and 6×10^6 g/mol polyacrylamide)^{34,36,67,69} while we found for PEO with a nominal initial molar weight of 4×10^6 g/mol in water $W > 15$.

V. RELATION BETWEEN M_w AND DR

Brostow predicted a linear correlation of M_n and DR .³⁶ As mentioned before, we concentrate on M_w instead of M_n since the data quality is significantly better. The measurements in the GPC were sometimes performed several days after the sample was drawn from ViEDRA. This time lack is considered for by an ageing correction with $b = 0.4$ when relating M_w and DR . The correlation of DR and ageing corrected $M_{w,a}$ is shown in [Fig. 8](#) for the experiments 4E6-1 and 4E6-2. 4E6-1 follows a linear dependence,

$$DR = 2.01 \times 10^{-7} M_{w,a} [\text{g/mol}] - 0.127. \quad (15)$$

This sets a lower threshold in $M_{w,a}$ of $\approx 630\,000$ g/mol to achieve DR . The $M_{w,a}$ threshold for drag reduction is even more pronounced in 4E6-2. In 4E6-2, the relation of DR and $M_{w,a}$ is not linear. This might be caused by a variation in polydispersity \mathcal{D} over distance and time [$\mathcal{D} = f(d, t_d)$] or the idea $DR \propto M_n$ is wrong. For $M_{w,a} \sim 2.5 \times 10^6$ g/mol DR in 4E6-2 is about twice the value in 4E6-1. This is worth mentioning since 4E6-2 is a repetition of 4E6-1. The main difference is the average number of runs per day which was higher for 4E6-2. The fact that the relation of DR and M_w differs so much between 4E6-1 and 4E6-2 points toward the need to consider the weight distribution instead of an average molar weight or to identify the weight fraction dominating DR . Already Hunston and Zakin³⁴ pointed out that the high molar weight tail in the molecular weight distribution might dominate DR . Our observation implies that the question raised by Soares³⁰

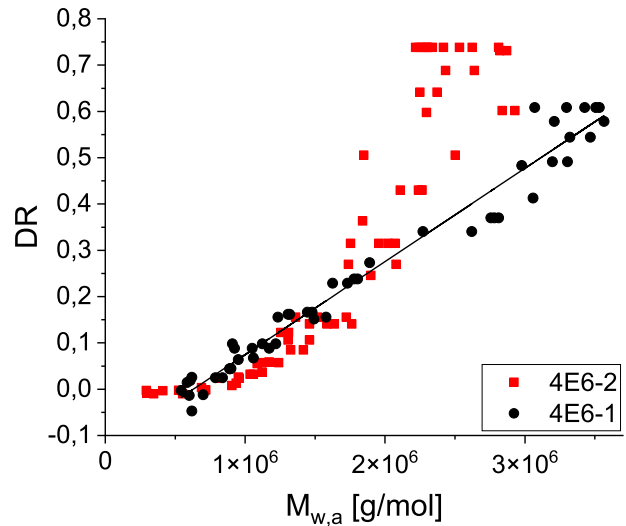


FIG. 8. DR in dependence of ageing corrected $M_{w,a}$ for datasets 4E6-1 and 4E6-2.

has to be broadened. Soares asked for a function F , which describes DR in dependence on the average molecular weight $M_{w,a}$,

$$\frac{DR}{DR_0} = F\left(\frac{M_{w,a}}{M_{w,a}(d=0)}\right), \quad (16)$$

while our data suggest that higher moments in the molecular weight distribution will influence DR . In fact, this is not unexpected since the molecular weight influences drag reduction in several ways. The wall shear stress at drag reduction onset scales with molecular weight as (Ref. 18) $T_w^{\text{onset}} \propto 1/M$. The slope of $1/\sqrt{f}$ over $\log Re\sqrt{f}$ in Prandtl-Karman coordinates scales differently with M . Virk¹⁸ derived for the slope increment $\tilde{\delta}$, which is a measure of drag reduction capability $\tilde{\delta} \propto M$. Different proportionalities on M in the scalings affecting DR will hardly be represented by $F(\frac{M_{w,a}}{M_{w,a}(d=0)})$.

VI. SUMMARY AND OUTLOOK

In this paper, we introduced the pilot-scale flow facility ViEDRA designed to investigate long-term drag reduction by polymers in turbulent pipe flows. Data of long-term experiments in 100 wppm aqueous PEO solutions at $Re = 10^5$ were presented. For a flow distance of ~ 10 km, a total loss of DR was observed. This DR loss was attributed to a reduction in the polymer chain length caused by shear degradation and ageing.

Ageing and degradation were assumed to be independent statistical processes and the M_w development in the turbulent flow was described empirically by Brostow's model modified by introduction of a decay term representing ageing. This fit function was successfully applied to describe the experimental data. For the number of breaking points of PEO chains with a nominal initial $M_w = 4 \times 10^6$ g/mol, a lower boundary can be given, which is about $W = 15$ for the experiments presented. For the residual molecular weight of the polymers at the end of the mechanical degradation, Brostow's model predicts a lower boundary of ~ 4100 g/mol in our experimental setting.

On the basis of our data, we see that DR increases with M , but we cannot verify the widely used assumption that $DR \propto M$ or the

existence of another unique function $DR = f(M)$. It seems to be more likely that higher-order moments in the mass distribution might determine DR as discussed by e.g., Hunston.³⁴

For PEO in water, we can clearly state that there is no remaining DR at infinite time. In our experiment, we could not observe that shear-induced polymer degradation in turbulent pipe flow ends before the polymer chain is fragmented into oligomers (less than ~ 100 repeat units). Fitting our data with the Brostow model indicated a lower limit of ~ 100 repeat units when mechanical degradation ends. However, this still has to be proven in future experiments. Ageing as well as degradation processes have to be investigated in more detail. From the modeling perspective, it is important to figure out if ageing and degradation can be treated independently.

SUPPLEMENTARY MATERIAL

See the [supplementary material](#) for further details on the methodology of the GPC and rheometer measurements, the generation of the reference data to calculate DR , on the fitting performance, and the ageing mechanism.

ACKNOWLEDGMENTS

H.W.M. appreciated the contributions of Andreas Stühler, MSc., and Lukas Bogner, BSc., to the characterization of polymer ageing, Konstantin Alge, BSc., and Jan-Luca Stampf, BSc., for their support in running the long-term experiments in ViEDRA and measuring samples taken from ViEDRA in the rheometer. All authors especially acknowledge the help of Emina Muratspahic, MEng. Her support was essential when installing ViEDRA, and she was always supportive when we needed help in operating ViEDRA, rheometer, or GPC. She provided valuable input for the rheological test procedures.

The authors are grateful for the financial support by the Institute of Materials Chemistry & Research, University of Vienna, Austria (Grant No. 3713000). L.B. acknowledges support of Doctoral College Advanced Functional Materials (DCAFM) funded by the Austrian Science Fund (FWF, Grant No.: DOC 85 doc. funds).

AUTHOR DECLARATIONS

Conflict of Interest

The authors have no conflicts to disclose.

Author Contributions

Hans Werner Müller redesigned the test facility ViEDRA and its software in preparation of the long-term experiments. All authors contributed to the experiment concept. Most of the experiments were performed by Lukas Brandfellner. The data evaluation was done by Lukas Brandfellner with contributions of Hans Werner Müller who provided all ageing and degradation fits presented. The work was supervised by Alexander Bismarck and Hans Werner Müller. Hans Werner Müller wrote the manuscript and the figures were prepared by Lukas Brandfellner and Hans Werner Müller. All authors reviewed and edited the manuscript.

Hans Werner Müller: Conceptualization (equal); Investigation (supporting); Methodology (supporting); Software (equal); Supervision (equal); Validation (supporting); Visualization (supporting); Writing –

original draft (lead); Writing – review & editing (equal). **Lukas Brandfellner:** Conceptualization (equal); Data curation (lead); Investigation (lead); Methodology (lead); Software (equal); Validation (lead); Visualization (lead); Writing – review & editing (equal). **Alexander Bismarck:** Conceptualization (equal); Resources (lead); Supervision (equal); Validation (supporting); Writing – review & editing (equal).

DATA AVAILABILITY

The data that support the findings of this study are available from the corresponding author upon reasonable request.

REFERENCES

- E. D. Burger, L. G. Chorn, and T. K. Perkins, "Studies of drag reduction conducted over a broad range of pipeline conditions when flowing Prudhoe bay crude oil," *J. Rheol.* **24**, 603–626 (1980).
- B. Yang, J. Zhao, J. Mao, H. Tan, Y. Zhang, and Z. Song, "Review of friction reducers used in slickwater fracturing fluids for shale gas reservoirs," *J. Nat. Gas Sci. Eng.* **62**, 302–313 (2019).
- A. G. Fabula, "Fire-fighting benefits of polymeric friction reduction," *J. Basic Eng.* **93**, 453–455 (1971).
- R. P. Singh, J. Singh, S. R. Deshmukh, D. Kumar, and A. Kumar, "Application of drag-reducing polymers in agriculture," *Curr. Sci.* **68**, 631–641 (1995).
- S. Phukan, P. Kumar, J. Panda, B. Nayak, K. Tiwari, and R. Singh, "Application of drag reducing commercial and purified guar gum for reduction of energy requirement of sprinkler irrigation and percolation rate of the soil," *Agric. Water Manage.* **47**, 101–118 (2001).
- M. F. Khalil, S. Z. Kassab, A. A. Elmilguy, and F. A. Naoum, "Applications of drag-reducing polymers in sprinkler irrigation systems: Sprinkler head performance," *J. Irrig. Drain. Eng.* **128**, 147–152 (2002).
- M. Poreh and U. Paz, "Turbulent heat transfer to dilute polymer solutions," *Int. J. Heat Mass Transfer* **11**, 805–818 (1968).
- M. Varnaseri and S. Peyghambarzadeh, "The effect of polyacrylamide drag reducing agent on friction factor and heat transfer coefficient in laminar, transition and turbulent flow regimes in circular pipes with different diameters," *Int. J. Heat Mass Transfer* **154**, 119815 (2020).
- W. Gong, J. Shen, W. Dai, K. Li, and M. Gong, "Research and applications of drag reduction in thermal equipment: A review," *Int. J. Heat Mass Transfer* **172**, 121152 (2021).
- R. H. J. Sellin and M. Ollis, "Polymer drag reduction in large pipes and sewers: Results of recent field trials," *J. Rheol.* **24**, 667–684 (1980).
- M. V. Kameneva, "Microrheological effects of drag-reducing polymers *in vitro* and *in vivo*," *Int. J. Eng. Sci.* **59**, 168–183 (2012).
- K. Avila, D. Moxey, A. de Lozar, M. Avila, D. Barkley, and B. Hof, "The onset of turbulence in pipe flow," *Science* **333**, 192–196 (2011).
- L. F. Richardson, *Weather Prediction by Numerical Process* (Cambridge University Press, London, 1922).
- A. N. Kolmogorov, "The local structure of turbulence in incompressible viscous fluid for very large Reynolds numbers," *Dokl. Akad. Nauk SSSR* **30**, 299–303 (1941).
- G. H. Choueiri, J. M. Lopez, and B. Hof, "Exceeding the asymptotic limit of polymer drag reduction," *Phys. Rev. Lett.* **120**, 124501 (2018).
- B. A. Toms, "Some observations on the flow of linear polymer solutions through straight tubes at large Reynolds numbers," in *First International Congress on Rheology* (North Holland Publ. Co., Amsterdam, 1948), pp. 135–141.
- J. L. Lumley, "Drag reduction by additives," *Annu. Rev. Fluid Mech.* **1**, 367–384 (1969).
- P. S. Virk, "Drag reduction fundamentals," *AIChE J.* **21**, 625–656 (1975).
- P. S. Virk, H. S. Mickley, and K. A. Smith, "The ultimate asymptote and mean flow structure in toms' phenomenon," *J. Appl. Mech.* **37**, 488–493 (1970).
- D. Samanta, Y. Dubief, M. Holzner, C. Schäfer, A. N. Morozov, C. Wagner, and B. Hof, "Elasto-inertial turbulence," *Proc. Natl. Acad. Sci.* **110**, 10557 (2013).

- ²¹M. Tabor and P. G. de Gennes, "A cascade theory of drag reduction," *Europhys. Lett.* **2**, 519 (1986).
- ²²Y. Dubief, C. M. White, V. E. Terrapon, E. S. G. Shaqfeh, P. Moin, and S. K. Lele, "On the coherent drag-reducing and turbulence-enhancing behaviour of polymers in wall flows," *J. Fluid Mech.* **514**, 271–280 (2004).
- ²³I. Zadrazil, A. Bismarck, G. F. Hewitt, and C. N. Markides, "Shear layers in the turbulent pipe flow of drag reducing polymer solutions," *Chem. Eng. Sci.* **72**, 142–154 (2012).
- ²⁴V. Voulgaropoulos, I. Zadrazil, N. Le Brun, A. Bismarck, and C. N. Markides, "On the link between experimentally-measured turbulence quantities and polymer-induced drag reduction in pipe flows," *AIChE J.* **65**, e16662 (2019).
- ²⁵C. M. White, V. S. R. Somandepalli, and M. G. Mungal, "The turbulence structure of drag-reduced boundary layer flow," *Exp. Fluids* **36**, 62–69 (2004).
- ²⁶M. D. Graham, "Drag reduction and the dynamics of turbulence in simple and complex fluids," *Phys. Fluids* **26**, 101301 (2014).
- ²⁷L. Xi, "Turbulent drag reduction by polymer additives: Fundamentals and recent advances," *Phys. Fluids* **31**, 121302 (2019).
- ²⁸V. Terrapon, Y. Dubief, P. Moin, E. S. Shaqfeh, and S. K. Lele, "Simulated polymer stretch in a turbulent flow using Brownian dynamics," *J. Fluid Mech.* **504**, 61–71 (2004).
- ²⁹C. M. White and M. G. Mungal, "Mechanics and prediction of turbulent drag reduction with polymer additives," *Annu. Rev. Fluid Mech.* **40**, 235–256 (2008).
- ³⁰E. J. Soares, "Review of mechanical degradation and de-aggregation of drag reducing polymers in turbulent flows," *J. Non-Newtonian Fluid Mech.* **276**, 104225 (2020).
- ³¹H. G. Sim, B. Khomami, and R. Sureshkumar, "Flow-induced chain scission in dilute polymer solutions: Algorithm development and results for scission dynamics in elongational flow," *J. Rheol.* **51**, 1223–1251 (2007).
- ³²A. F. Horn and E. W. Merrill, "Midpoint scission of macromolecules in dilute solution in turbulent flow," *Nature* **312**, 140–141 (1984).
- ³³J. A. Odell, A. Keller, and Y. Rabin, "Flow-induced scission of isolated macromolecules," *J. Chem. Phys.* **88**, 4022–4028 (1988).
- ³⁴D. L. Hunston and J. L. Zakin, "Flow-assisted degradation in dilute polystyrene solutions," *Polym. Eng. Sci.* **20**, 517–523 (1980).
- ³⁵N. S. Berman, "Drag reduction by polymers," *Annu. Rev. Fluid Mech.* **10**, 47–64 (1978).
- ³⁶W. Brostow, "Drag reduction and mechanical degradation in polymer solutions in flow," *Polymer* **24**, 631–638 (1983).
- ³⁷E. J. Soares, G. A. B. Sandoval, L. Silveira, A. S. Pereira, R. Trevelin, and F. Thomaz, "Loss of efficiency of polymeric drag reducers induced by high Reynolds number flows in tubes with imposed pressure," *Phys. Fluids* **27**, 125105 (2015).
- ³⁸M. Mohammadtabar, R. Sanders, and S. Ghaemi, "Viscoelastic properties of flexible and rigid polymers for turbulent drag reduction," *J. Non-Newtonian Fluid Mech.* **283**, 104347 (2020).
- ³⁹Y. Gu, S. Yu, J. Mou, D. Wu, and S. Zheng, "Research progress on the collaborative drag reduction effect of polymers and surfactants," *Materials* **13**, 444 (2020).
- ⁴⁰M. Asidin, E. Suali, T. Jusnukin, and F. Lahin, "Review on the applications and developments of drag reducing polymer in turbulent pipe flow," *Chin. J. Chem. Eng.* **27**, 1921–1932 (2019).
- ⁴¹M.-H. Wei, B. Li, R. L. A. David, S. C. Jones, V. Sarohia, J. A. Schmitgal, and J. A. Kornfield, "Megasupramolecules for safer, cleaner fuel by end association of long telechelic polymers," *Science* **350**, 72–75 (2015).
- ⁴²E. Muratpahić, L. Brandfellner, J. Schöffmann, A. Bismarck, and H. W. Müller, "Aqueous solutions of associating poly(acrylamide-co-styrene): A path to improve drag reduction?," *Macromolecules* **55**, 10479 (2022).
- ⁴³T. Nakken, M. Tande, and A. Elgsaeter, "Measurements of polymer induced drag reduction and polymer scission in Taylor flow using standard double-gap sample holders with axial symmetry," *J. Non-Newtonian Fluid Mech.* **97**, 1–12 (2001).
- ⁴⁴J. H. Sung, C. A. Kim, H. J. Choi, B. K. Hur, J. G. Kim, and M. S. Jhon, "Turbulent drag reduction efficiency and mechanical degradation of poly(acrylamide)," *J. Macromol. Sci., Part B* **43**, 507–518 (2004).
- ⁴⁵A. S. Pereira and E. J. Soares, "Polymer degradation of dilute solutions in turbulent drag reducing flows in a cylindrical double gap rheometer device," *J. Non-Newtonian Fluid Mech.* **179–180**, 9–22 (2012).
- ⁴⁶C. H. Hong, H. J. Choi, K. Zhang, F. Renou, and M. Grisel, "Effect of salt on turbulent drag reduction of xanthan gum," *Carbohydr. Polym.* **121**, 342–347 (2015).
- ⁴⁷A. Rajappan and G. H. McKinley, "Epidermal biopolysaccharides from plant seeds enable biodegradable turbulent drag reduction," *Sci. Rep.* **9**, 18263 (2019).
- ⁴⁸W. R. dos Santos, E. Spalenza Caser, E. J. Soares, and R. N. Siqueira, "Drag reduction in turbulent flows by diutan gum: A very stable natural drag reducer," *J. Non-Newtonian Fluid Mech.* **276**, 104223 (2020).
- ⁴⁹R. W. Paterson and F. H. Abernathy, "Turbulent flow drag reduction and degradation with dilute polymer solutions," *J. Fluid Mech.* **43**, 689–710 (1970).
- ⁵⁰W. Interthal and H. Wilski, "Drag reduction experiments with very large pipes," *Colloid Polym. Sci.* **263**, 217–1536 (1985).
- ⁵¹J. M. J. den Toonder, A. A. Draad, G. D. C. Kuiken, and F. T. M. Nieuwstadt, "Degradation effects of dilute polymer solutions on turbulent drag reduction in pipe flows," *Appl. Sci. Res.* **55**, 63–82 (1995).
- ⁵²N. Le Brun, I. Zadrazil, L. Norman, A. Bismarck, and C. N. Markides, "On the drag reduction effect and shear stability of improved acrylamide copolymers for enhanced hydraulic fracturing," *Chem. Eng. Sci.* **146**, 135–143 (2016).
- ⁵³X. Zhang, X. Dai, J. Zhao, D. Jing, F. Liu, L. Li, Y. Xin, and K. Liu, "Precise prediction of the drag reduction efficiency of polymer in turbulent flow considering diameter effect," *Phys. Fluids* **33**, 095124 (2021).
- ⁵⁴M. Habibpour and P. E. Clark, "Drag reduction behavior of hydrolyzed polyacrylamide/xanthan gum mixed polymer solutions," *Pet. Sci.* **14**, 412–423 (2017).
- ⁵⁵P. Alexandridis, "Amphiphilic copolymers and their applications," *Curr. Opin. Colloid Interface Sci.* **1**, 490–501 (1996).
- ⁵⁶S. Kirinčić and C. Klofutar, "Viscosity of aqueous solutions of poly(ethylene glycol)s at 298.15 K," *Fluid Phase Equilib.* **155**, 311–325 (1999).
- ⁵⁷I. Zadrazil, "Various aspects of polymer induced drag reduction in turbulent flow," Ph.D. thesis (Imperial College, 2011).
- ⁵⁸R. H. J. Sellin, J. W. Hoyt, and O. Scrivener, "The effect of drag-reducing additives on fluid flows and their industrial applications—Part 1: Basic aspects," *J. Hydraul. Res.* **20**, 29–68 (1982).
- ⁵⁹Y. A. Cengel and J. M. Cimbala, "Flow in pipes," in *Fluid Mechanics: Fundamentals and Applications* (McGraw-Hill Higher Education, 2006), pp. 321–398.
- ⁶⁰D. Held and P. Kilz, "Qualification of GPC/GFC/SEC data and results," in *Quantification in LC and GC: A Practical Guide to Good Chromatographic Data*, edited by H.-J. Kuss and S. Kromidas (Wiley, 2009), pp. 271–302.
- ⁶¹F. Wendt, "Turbulente Strömungen zwischen zwei rotierenden konaxialen Zylindern," *Ing.-Arch.* **4**, 577–595 (1933).
- ⁶²J. M. J. Den Toonder, M. A. Hulsen, G. D. C. Kuiken, and F. T. M. Nieuwstadt, "Drag reduction by polymer additives in a turbulent pipe flow: Numerical and laboratory experiments," *J. Fluid Mech.* **337**, 193–231 (1997).
- ⁶³M. Polverari and T. G. M. van de Ven, "Dilute aqueous poly(ethylene oxide) solutions: Clusters and single molecules in thermodynamic equilibrium," *J. Phys. Chem.* **100**, 13687–13695 (1996).
- ⁶⁴C. Brennen and G. E. Gadd, "Aging and degradation in dilute polymer solutions," *Nature* **215**, 1368–1370 (1967).
- ⁶⁵Y. Layec and M.-N. Layec-Raphalen, "Instability of dilute poly(ethylene-oxide) solutions," *J. Phys. Lett.* **44**, 121–128 (1983).
- ⁶⁶C. W. McGary, Jr., "Degradation of poly(ethylene oxide)," *J. Polym. Sci.* **46**, 51–57 (1960).
- ⁶⁷W. Brostow, H. Ertepinar, and R. P. Singh, "Flow of dilute polymer solutions: Chain conformations and degradation of drag reducers," *Macromol.* **23**, 5109–5118 (1990).
- ⁶⁸W. Brostow, "Drag reduction in flow: Review of applications, mechanism and prediction," *J. Ind. Eng. Chem.* **14**, 409–416 (2008).
- ⁶⁹J. P. Malhotra, P. N. Chaturvedi, and R. P. Singh, "Shear stability studies on polymer-polymer and polymer-fibre mixtures," *Rheol. Acta* **26**, 31–39 (1987).